MACHINE VISION-BASED AREA CALCULATION METHOD FOR LASER CLADDING REGIONS ON ROTARY TILLER BLADES

/

基于机器视觉的旋耕刀片激光熔覆区域面积计算方法研究

Yifan HOU[1,2)], Juan FENG[1,2)], Hao BAI[1)], Siying LIU[1)], Hongling JIN[*3)] [1]

[1)]Xi'an Aeronautical Polytechnic Institute, Shaanxi Xi'an 710089;
[2)]Shaanxi Higher Vocational College Key Laboratory of Aerospace Fastener Technology and Application, Xi'an Aeronautical Polytechnic Institute, Shaanxi Xi'an 710089,
[3)]Northwest A&F University College of Mechanical and Electronic Engineering, Shaanxi Yangling 712100
Tel: +86 18729002242; E-mail addresses: houyifan@nwafu.edu.cn
Corresponding author: Hongling Jin
DOI: https://doi.org/10.35633/inmateh-77-67

Keywords: *Machine vision, agricultural machinery, laser cladding, irregular area measurement, quality inspection*

ABSTRACT

To address the challenges of irregular morphology and the difficulty in rapidly and accurately measuring the area of laser cladding zones during the inspection of agricultural rotary tiller blades, this paper proposes a machine vision-based method for rapid area extraction. A comprehensive processing workflow encompassing image preprocessing, contour extraction, region of interest (ROI) extraction, and pixel integration was established. For region segmentation, an improved Alpha Shapes segmentation algorithm was proposed and compared against conventional Convex Hull and Delaunay triangulation methods. Validation was conducted using 100 rotary tiller blade samples, with electron microscopy manual calibration results serving as reference. Results indicate the improved Alpha Shapes algorithm delivers optimal segmentation accuracy, yielding the smallest absolute area error ($-7.40\times10^{-7} \pm 2.69\times10^{-5}$)m² and lowest relative error $(13.48 \pm 8.47)\times10^{-3}$, with high consistency against microscopic measurements. Compared to conventional manual measurement, the area extraction algorithm proposed in this study offers the advantages of automation, non-contact operation, and high efficiency, meeting the engineering application requirements for laser cladding quality inspection.

摘要

针对农用旋耕刀片检测中激光熔覆区域形态不规则、面积难以快速准确测量的问题，本文提出了一种基于机器视觉的面积快速提取方法。构建了包含图像预处理、轮廓提取、ROI提取与像素积分的完整处理流程。在区域分割时，提出了一种改进的Alpha Shapes区域分割算法，将其与常用Convex Hull与Delaunay剖分合并两种算法进行对比，试验选取100个旋耕刀片样本进行验证，以电子显微镜人工标定结果为参考。结果表明，改进的Alpha_shape算法在区域分割精度上表现最佳，最终计算面积绝对误差最小（$-7.40\times10^{-7} \pm 2.69\times10^{-5}$)m²、相对误差最低$(13.48 \pm 8.47)\times10^{-3}$且与显微镜测量结果高度一致。与传统人工测量相比，本研究提出的面积提取算法具有自动化、非接触和高效的优势，满足激光熔覆质量检测的工程应用需求。

INTRODUCTION

As a critical component of agricultural rotary tillers, rotary tiller blades operate under complex conditions where their cutting edges endure significant impact. Laser cladding is frequently employed to enhance edge durability. This manufacturing technique utilizes a high-power laser beam to melt metal powder and fuse it with the substrate, thereby improving surface hardness, corrosion resistance, and wear resistance (*Hou et al., 2025; Poloczek et al., 2022; Ding Y. et al, 2022*). During production inspection, the laser cladding area serves as a critical indicator influencing the strengthening effect, directly impacting the product's wear resistance and service life *(Zhu, 2018)*. Consequently, its precise measurement is essential. However, the complex geometry of rotary tiller blade edges and the irregular shape of the cladding zone render traditional measurement methods—such as manual calibration via electron microscopy or estimation using gauges—cumbersome, inefficient, and lacking in accuracy, rendering them unsuitable for mass inspection requirements (*Zhang Y. et al, 2025; Haldar and Saha, 2018*).

[1] *Yifan Hou, Lecturer, M.S. Stud. Eng.; Juan Feng, Prof. M.S. Stud. Eng.; Hao Bai, B.Eng.; Siying Liu, M.S. Stud. Eng.; Hongling Jin*, Prof. Ph.D. Eng.*

This paper proposes a machine vision-based method for the rapid extraction of irregular cladding areas on rotary tiller blades, aiming to improve the automation and precision of blade inspection. In terms of irregular region extraction, an optimal balance between compression ratio and information retention was achieved through a novel irregular-shape extraction scheme (*Li, 2007*). An automatic extraction approach for regions of interest in shallow depth-of-field images was developed, enabling the separation of foreground regions of interest from non-essential background areas to support irregular shape extraction (*Minchul and Hong, 2010*). A two-dimensional image analysis framework based on saliency maps was introduced, where salient regions are identified via topological transformations and dynamic neural networks to extract pixels with the highest saliency values as regions of interest (*Itti and Koch, 1999*). Additionally, a machine vision method for estimating object volume and surface area was proposed, in which multi-angle profiles are acquired through object rotation, followed by three-dimensional reconstruction via edge-point extraction, allowing accurate area calculation of arbitrary object regions (*Lee et al., 2006*).

Compared to irregular regions in natural scenes or conventional workpiece surfaces, laser cladding zones exhibit smooth, highly reflective metal surfaces with uneven grey-scale distribution and blurred boundary transitions. This renders traditional region extraction algorithms—based on saliency maps, shallow depth of field, or 3D reconstruction—unstable in boundary detection and computationally complex for such images, failing to meet real-time and accuracy requirements. To address these challenges, this paper proposes a machine vision algorithm for area extraction in laser-clad regions of rotary tiller blades. Its key innovations include:

1. A comprehensive image-processing workflow is established.

Greyscale conversion, Gaussian blur noise reduction, OTSU automatic threshold segmentation, and morphological operations are combined to effectively suppress noise on highly reflective metal surfaces and enhance edge clarity. A contour-detection algorithm based on boundary tracking *(Yokoyama and Poggio, 2005)* is used to extract the blade's maximum closed contour and generate a mask for isolating the blade region. Grey-level analysis is applied to extract high-brightness regions and mitigate illumination effects. Furthermore, an ROI extraction mechanism based on grey-level analysis and density screening is designed to achieve adaptive recognition and illumination compensation for high-brightness laser-cladding regions.

2. An improved Alpha Shapes region-segmentation algorithm is proposed, introducing traditional point-cloud boundary detection concepts into the image domain

This approach significantly improves the accuracy and robustness of irregular cladding-boundary recognition. Comparative analyses with conventional Convex Hull and Delaunay triangulation segmentation algorithms demonstrate superior precision and efficiency. Experimental results confirm that the improved Alpha Shapes algorithm provides higher accuracy and stability in extracting irregular cladding areas, meeting the requirements of industrial applications.

MATERIALS AND METHODS

Image Preprocessing

The original image of the cutting blade (Figure.1-(a)) underwent preprocessing, primarily comprising greyscale conversion, noise reduction, binarization segmentation, and morphological processing (*Al-Khudhairy et al., 1983*). First, the color image was converted to greyscale to simplify and reduce computational complexity (Figure. 1-(b)). As the cladding substrate is metallic with numerous reflective areas, greyscaling introduced significant noise that impaired edge detection and contour extraction. Gaussian blurring was therefore employed for noise reduction (*Lubis and Iqbal, 2024*), achieving image smoothing through Gaussian weighted averaging (Figure. 1-(c)). To preliminarily extract the laser cladding region, the Otsu automatic threshold segmentation method is applied: Otsu employs grey-level histogram analysis, traversing all threshold values *t* based on the principle of maximizing inter-class variance. The threshold maximizing inter-class variance is selected to achieve foreground-background segmentation, generating a binary image (Figure. 1-(d)). The principle is illustrated in Equation 1:

$$\sigma^2{}_B(t) = \omega_0(t)\omega_1(t)[\mu_0(t) - \mu_1(t)]^2 \quad (1)$$

where $\omega_0(t)$ and $\omega_1(t)$ represent the normalized weights of the background and foreground at threshold t, and $\mu_0(t)$ and $\mu_1(t)$ denote their respective mean gray values.

OTSU processing resulted in the partial loss of detail within the cladding region. This study employed morphological closing operations to fill cavities within the cladding area and eliminate minor noise. The closing operation comprises dilation and erosion: dilation expands the foreground region, followed by erosion to restore boundaries.

The underlying principles are detailed in Equations 2 and 3.

$$\text{expansion processing: } A \oplus B = \{z|(B_z \cap A) \neq \emptyset\} \quad (2)$$

$$\text{corrosion treatment: } A - B = \{z|B_z \subseteq A\} \quad (3)$$

where A denotes the original image, B represents the structural element, and B_z indicates the sliding window of the structural element across the image.

Morphological operations effectively fill small voids and remove minor noise within irregular regions, resulting in smoother images with clearer and more continuous contours (Fig. 1-(e)).

Fig. 1 – (a) Blade original image; (b) Conversion of greyscale images; (c) Gaussian blur; (d) OTSU Automatic Threshold Segmentation; (e) Morphological closure operation

Blade Profile Extraction

During real-world operation testing, backgrounds are often complex. Rapid object boundary localization through blade contour extraction enhances detection accuracy and efficiency. This study employs boundary tracking on binary images for contour detection (*Ren et al., 2002*). The cv2.findContours() function in OpenCV is utilized to extract regional boundaries. Based on the characteristics of rotary tiller blade imagery, the largest contour is selected as the blade region boundary by comparing contour areas (Figure. 2-(a)). Let all extracted contours be denoted as $C_1, C_2 ..... C_n$ where n represents the total number of contours. Each contour C_i comprises a set of points. The contour area $A(C_i)$ can be obtained by calculating the number of internal pixels, as expressed in Equation 4:

$$A(C_i) = \sum_{x,y \in C_i} I(x,y) \quad (4)$$

Here, $I(x,y)$ represents the value of a pixel at coordinates (x,y) in the image.

After selecting the contour of the rotary tiller blade, an object mask is generated based on its shape. This mask is a binarized image matching the dimensions of the original image (*Lv et al 2022; Zeng et al., 2021*). The mask image is defined as $M(x,y)$, where $M(x,y)=1$ denotes the target object and $M(x,y)=0$ represents the background. The mask M is generated by applying the maximum contour C_{max} to a fully zeroed image, rendering the target region white, with the background remaining black (Figure. 2-(b)). This mask enables extraction of the blade region's grey-scale information. Let the original image's grey-scale value be $G(x,y)$.

The grey-scale information of the target region is obtained by performing a bitwise AND operation between the mask $M(x,y)$ and the original image, as expressed in Equation 5:

$$G_{obj}(x,y) = G(x,y) \cdot M(x,y) \quad (5)$$

where: $G_{obj}(x,y)$ denotes the grey value within the blade region, with grey values in other regions set to zero. Extracting the grey-scale distribution of the blade area (Figure. 2-(c)) lays the groundwork for subsequent brightness analysis and region detection.

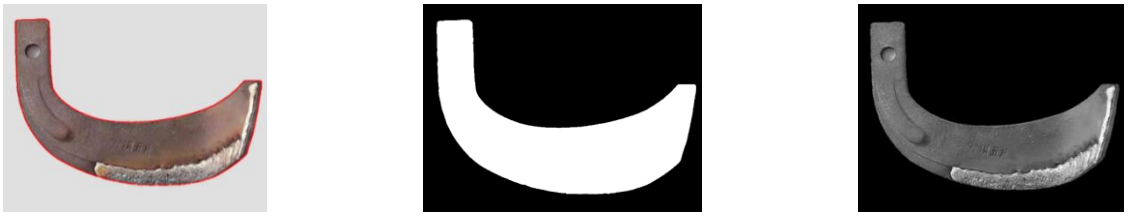

Fig. 2 – (a) Maximum area contour; (b) Mask processing;
(c) Extract grayscale information from the object region

Extraction of the Cladding ROI

In greyscale images, laser cladding regions tend to exhibit high brightness due to factors such as illumination and material properties. This study employs a greyscale histogram analysis algorithm (*Liu, 2024*) to segment these bright areas using a fixed threshold, thereby optimizing regional recognition accuracy. Higher greyscale values indicate greater brightness. If the grey value $G(x,y)$ of an image pixel exceeds the set threshold T_{High}, that pixel belongs to the bright region. For each pixel (x,y) in an image, the extraction of bright regions can be determined using Equation 6:

$$G_{bright}(x,y) = \begin{cases} G(x,y), & if G(x,y) > T_{htgh} \\ 0, otherwise \end{cases} \tag{6}$$

Here, $G_{bright}(x,y)$ represents the extracted high-intensity region image; $G(x,y)$ denotes the grayscale values of the original image; and T_{high} is the threshold for defining high-intensity regions. By extracting all pixels with brightness exceeding the specified threshold, the high-intensity cladding regions are obtained (Fig. 3-(a)).

To further eliminate isolated noise points while preserving bright regions exhibiting spatially clustered characteristics, this study introduces a local density threshold screening mechanism based on the luminance binary image. By employing a sliding window to statistically analyze the density distribution of bright pixels within local regions, it determines whether an area constitutes a significantly clustered solder joint region. Let the binary image of the bright region be denoted as $B_f(x,y) \in \{0,255\}$ It is first normalized into a floating-point image:

$$B_f(x,y) = \frac{B(x,y)}{255} \in \{0,1\} \tag{7}$$

Then, a sliding window is applied to compute the integral average over the neighborhood of each pixel, resulting in the local density map $D(x,y)$:

$$D(x,y) = \frac{1}{K^2} \sum_{i=-k}^{k} \sum_{j=-k}^{k} B_f(x+i, y+j) \tag{8}$$

Here, $K \times K$ denotes the kernel window size. This process may be understood as calculating the proportion of “white points” within each pixel neighborhood, thereby estimating their spatial density.

To eliminate regions of excessively low density, a global density threshold T is set:

$$T = \tau \cdot \max_{x,y} D(x,y) \tag{9}$$

Here, τ is the density threshold coefficient, which is set to 0.03 in this study. Density screening is performed using Formula (10).

$$B_{filt}(x,y) = \begin{cases} 0 & D(x,y) < T \\ B(x,y) & D(x,y) \geq T \end{cases} \tag{10}$$

Fig. 3 – (a) Highlighted Area Extraction; (b) Density Screening Region of Interest

Region Segmentation

Based on the preceding image preprocessing framework, this study proposes a region segmentation method, namely an improved Alpha Shapes model, and conducts comparative validation using multiple representative segmentation algorithms. Common region segmentation methods mainly include deep learning-based models such as U-Net, as well as geometry-driven algorithms such as Active Contours, Convex Hull, and Delaunay triangulation-based region merging.

Deep learning-based methods usually rely on large-scale, high-precision pixel-level annotated datasets, which involve high data acquisition costs. In contrast, the recognition scenario of laser-cladded regions on rotary tiller blades is relatively specific, where low cost, stability and engineering applicability are of greater importance. Therefore, this study primarily focuses on geometry-constrained segmentation methods. Active contour models are driven by image gradient information and perform iterative curve evolution, which are more suitable for continuous grayscale boundary structures. In this study, the images have been transformed into a binary form through the preprocessing stage and exhibit explicit geometric boundary characteristics, under which the application of such iterative evolution mechanisms may introduce additional boundary disturbances (*Chan and Vese, 2001)*. The Convex Hull algorithm is adopted as an efficient and stable baseline method, with good adaptability to binary images, while the Delaunay triangulation-based region merging method represents a classical topology-driven reconstruction strategy. Based on the above considerations, this study selects the improved Alpha Shapes, Convex Hull, and Delaunay triangulation-based region merging methods for comparative experimental evaluation.

1) Improved Alpha Shapes Algorithm

The Alpha Shapes algorithm, renowned for its high accuracy and efficiency, is frequently employed for boundary extraction and projected area calculation in lidar point clouds (*Edelsbrunner et al.,1983*). However, its direct application in image processing is hindered by the lack of suitable input point sets. This study proposes an improved Alpha Shapes algorithm to extend its applicability to the image domain. It begins by extracting coordinates from non-zero pixels within high-brightness regions of acquired laser cladding images, filtering their areas, and consolidating them into a two-dimensional point set. These points constitute an 'image point set' equivalent to the point cloud structure, with boundary points serving as the algorithm's input. The algorithm employs a rolling circle with an adjustable radius that traverses the boundary points. When the radius α is appropriately chosen, the circle rolls exclusively along the boundary points, tracing the contour of the graphic region (Figure. 4). The algorithmic steps are as follows:

(1) The rolling circle radius α is adaptively determined through the spatial distribution of boundary pixels. For the two-dimensional point set P within the cladding region, the median nearest neighbor distance is calculated for any point $p_i(x_i,y_i)$ and used as the initial radius. Subsequently, an appropriate α value is obtained by adjusting for image region area stability, employing the following algorithm:

$$\alpha_0 = median\left(\min_{j\neq i}\|pi - pj\|\right) \tag{11}$$

$$\alpha = \lambda\alpha_0, \lambda \in [1,2] \tag{12}$$

where: λ denotes the median nearest neighbor distance, with the scaling factor λ determined through discrete stability search.

(2) Search within the point cloud for all points within *α* distance of less than 2α from point p, denoted as point set Q;

(3) Select any point $P(x,y)$ from the point set Q, and, based on points P,P_1, and the rolling circle radius α, calculate the coordinates of two circle centers, $Q_1(x_{o1},y_{o1})$ and $Q_2(x_{o2},y_{o2})$, The calculation formulas for the circle centers O_1 and O_2 are as follows:

$$\begin{aligned} &①x_{o2} = x + \frac{1}{2}(x_1 - x) + H*(y_1 - y); \quad ②x_{o1} = x + \frac{1}{2}(x_1 - x) - H*(y_1 - y) \\ &③y_{o1} = y + \frac{1}{2}(y_1 - y) - H*(x - x_1); \quad ④y_{o2} = y + \frac{1}{2}(y_1 - y) + Hl*(x - x_1) \end{aligned} \tag{13}$$

Where: $H = \sqrt{\frac{a^2}{S^2} - \frac{1}{4}}$; $S^2 = (x - x_1)^2 + (y - y_1)^2$.

(4) For each point in the point set Q other than point P_1, calculate its distance to the centers O_1 and O_2 respectively. If the distance exceeds α, mark the point P as a contour point.

(5) If the distances from all other points in set Q (excluding P_1) to the circle centers O_1 and O_2 are not all greater than α, then iterate through all points in Q, each serving in turn as point P_1, and recalculate the circle centers. Apply the procedure in step (3) to determine the status of point P. If there exists a point that causes P to be marked as a contour point, it is classified as a contour point, otherwise, it is considered a non-contour point.

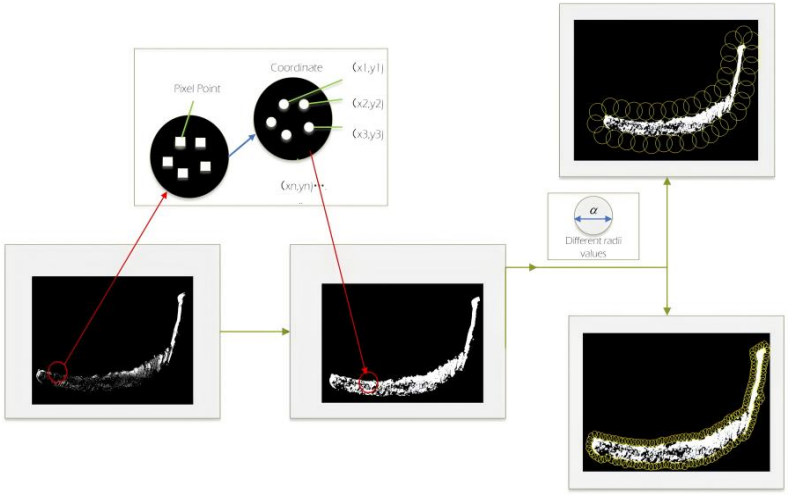

Fig. 4–Improved Alpha Shapes algorithm

2) Convex Hull Algorithm

A Convex Hull is a method for describing the tightest enclosing shape of a graph's external boundary. Given a set of points S, its Convex Hull is the smallest convex polygon that encompasses the set S. This study employs the Graham scan algorithm *(Kong et al., 1990)* for two-dimensional Convex Hull computation. It sorts the acquired high points by polar angle, then uses vector cross products to determine 'direction changes' before retaining or discarding points, sequentially constructing a counter-clockwise Convex Hull boundary. Given three consecutive points, they are defined as two vector segments:

$$\vec{v}_2 = \overrightarrow{p_j p_k} = (x_k - x_j, y_k - y_i) \tag{14}$$

Compute the two-dimensional vector cross product of these vectors:

$$\vec{v}_1 \times \vec{v}_1 = (x_j - x_i)(y_k - y_j) - (y_j - y_i)(x_k - x_j) \tag{15}$$

If the cross product is greater than zero, it indicates that the path from $P_i \rightarrow P_j \rightarrow P_k$ constitutes a left turn and forms part of the Convex Hull. If the cross product≤0, it represents a right turn or collinearity, and the intermediate point P_i should be removed. By progressively scanning the surface and applying the aforementioned polar angle sorting and cross-product test, the boundary defining the Convex Hull is ultimately determined.

3) Delaunay partitioning and merging

This algorithm employs Delaunay (*Lee et al, 1986*) triangulation to partition the laser cladding region and merge it to extract continuous targets. The fundamental condition for triangulation is that no other point may lie within the circumscribed circle of any triangle; this is termed the circumscribed circle condition. Given a triangle ABC and a point P, if point P lies within the circumscribed circle of triangle ABC, then that triangle fails to satisfy the Delaunay property and should be replaced or re-partitioned. The verification formula is:

$$\begin{vmatrix} x_A & y_A & x^2{}_A + y^2{}_A & 1 \\ x_B & y_B & x^2{}_B + y^2{}_B & 1 \\ x_C & y_C & x^2{}_C + y^2{}_C & 1 \\ x_p & y_P & x^2{}_P + y^2{}_P & 1 \end{vmatrix} \quad (16)$$

Here, are (x_A,y_A), (x_B,y_B), (x_C,y_C) the three vertices of triangle ABC, and (x_p,y_p) represents the point P to be tested.

If the result is greater than zero, point P lies outside the circumscribed circle and satisfies Delaunay properties, thus qualifying for partitioning. If the result equals zero, P lies on the circumscribed circle. If the result is less than zero, Delaunay properties are violated, indicating P lies inside the circumscribed circle. Next, the areas of all triangles Δi generated by the triangulation are analyzed. An area threshold ε is defined. Any triangle with area $S_i<\varepsilon$, is considered a noise-induced small face and is removed. If adjacent small triangles satisfy topological adjacency (i.e., share a common edge), they may be merged into a single polygon based on their shared boundary. After merging, the total area S_{total} of the combined region is calculated.

Area Calculation

This study employs the grid method for area calculation. Within the discrete grid model, all partitioned pixels are traversed to perform area accumulation operations, with the algorithm detailed in Equation 17.

$$A = \sum_{(x,y)\in P_{inside}} 1 \quad (17)$$

where: P_{inside} denotes all pixels within the laser cladding zone.

The raw image captured during imaging comprises pixels, which must undergo pixel calibration to convert pixel counts into area measurements (*Song, 2022*). The conversion formula is shown in Eq. 18:

$$A_{real} = A_{pixel} \times \frac{1}{n} \sum_{i=1}^{n} \frac{A_{i,SEM}}{A_{i,pixel}} \quad (18)$$

where: A_{real} denotes the area extracted by machine vision; A_{pixel} denotes the pixel area extracted by machine vision; $A_{i,SEM}$ denotes the true area of a sample calibrated manually; $A_{i,pixel}$ denotes the pixel area of a sample. Selecting n=10 yields the single-pixel area value used in this study as $3.78\times10^{-8}m^2$. Based on this, the area from each blade to the cladding region may be calculated.

RESULTS

This experiment compared the accuracy and efficiency of three different region extraction algorithms in the region segmentation stage: the improved Alpha Shapes algorithm, the Convex Hull method, and the Delaunay triangulation method. One hundred rotary tiller blades were selected as samples. Machine vision images were acquired using an industrial camera platform (Figure 5), with specific parameters shown in Table 1. Illumination was achieved using an LED ring light installed directly above the blade samples at an incident angle of 0°, with a power of 20 W and an illumination intensity maintained at approximately 2000–2500 lux to minimize specular reflection while preserving brightness contrast within the laser cladding area.

Fig. 5 – Industrial Camera Platform

Table 1

Industrial Camera Specifications

Parameter Name	Specification/Value
Sensor Model	Sony IMX178
Pixel size	2.4 μm x 2.4 μm
Resolution	3072x2048
Signal-to-noise ratio	41.3 dB
Exposure time	52 μs ~ 10s
Data Interface	Gigabit Ethernet (1000Mbits)

The control group measured the actual area of reference specimens via manual calibration using an electron microscope (Figure. 6), with key parameters detailed in Table 2.

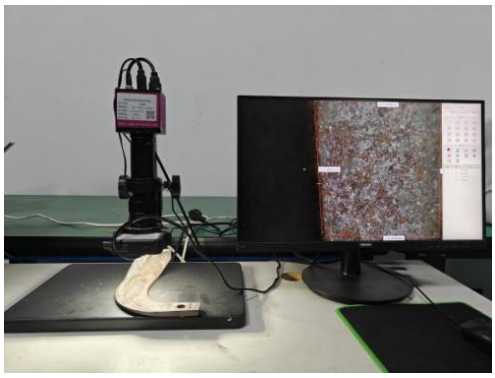

Fig. 6 - Electron microscope calibration area

Table 2

Electron Microscope Parameters

Parameter Name	Specification/Value
Model	JSM-IT500HR
Magnification	10×-500,000×
resolution	1.0nm(15kV)
Working distance	5mm-48mm
Signal Acquisition Mode	backscattered electrons/X-ray energy spectrum
Data output format	TIFF, JPEG, BMP

During the regional segmentation phase, three distinct algorithms - improved Alpha Shapes, Convex Hull, and Delaunay triangulation - were employed to extract visualized results, as depicted in Figure 7.

Fig. 7 – (a) Improved Alpha Shapes; (b) Convex Hull; (c) Delaunay partitioning and merging

The areas extracted using the three methods were all recorded and compared with the manually calibrated measured areas. The resulting scatter plots and box plots are shown in Figures 8 and 9.

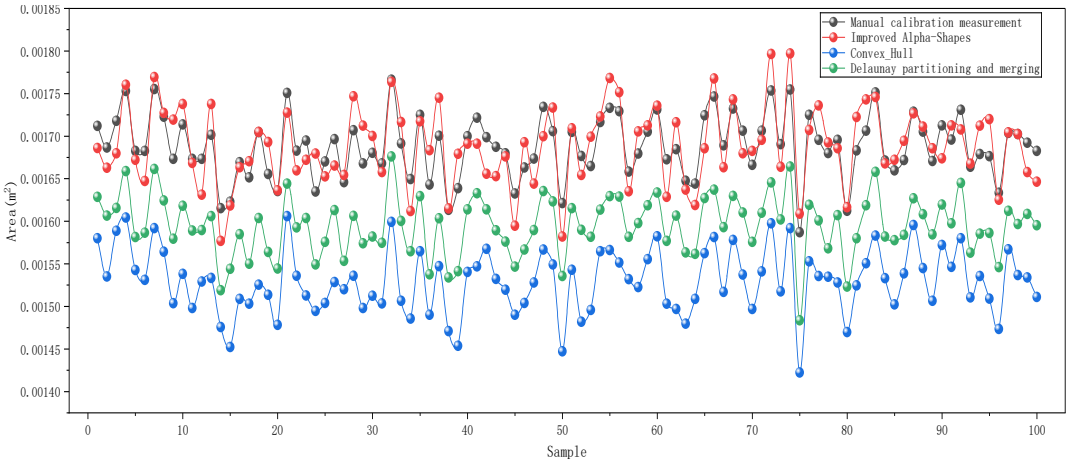

Fig. 8 – Scatter plot

Figure 8 demonstrates that the area estimation results from the three methods exhibit significant discrepancies across different samples, with the improved Alpha Shapes algorithm delivering superior accuracy and stability in extracted area values.

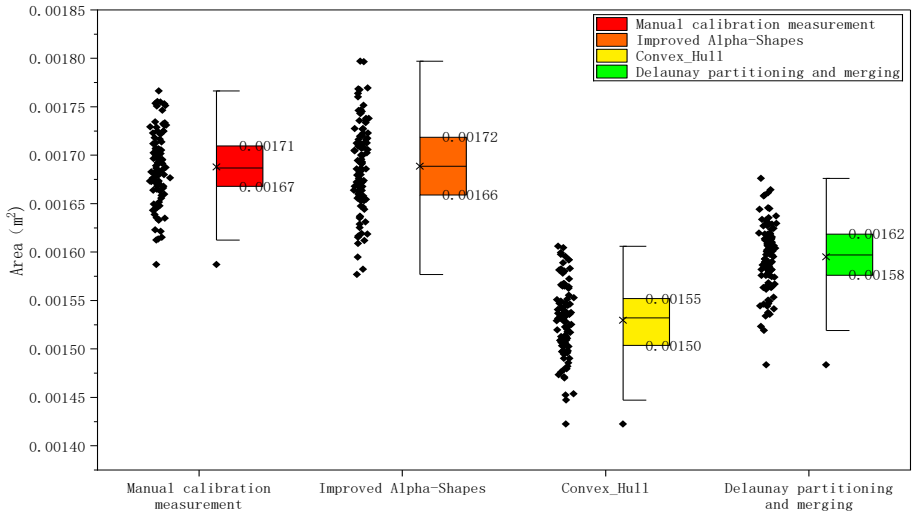

Fig. 9 – Box plot

The box plot in Figure 9 shows that the median values are very close to the true values, with a symmetrical distribution and no noticeable bias. In contrast, the Convex Hull method exhibits significant underestimation, while the Delaunay triangulation-based merging method yields intermediate estimates that are still generally smaller than the true values.

To quantitatively analyze the accuracy and timeliness of area extraction across three methods, the absolute error $\mathfrak{E}_{abs}$ and relative error $\mathfrak{E}_{rel}$ metrics were calculated using Equations 19 and 20. These metrics were employed to evaluate the accuracy of area acquisition. The mean error, standard deviation, and 95% confidence interval were computed for each algorithm, alongside recording the time taken for each extraction. The data were imported into the statistical analysis software SPSS for evaluation, with the results presented in the table 3 below.

$$\varepsilon_{abs} = \left| A_{ex} - A_{true} \right| \tag{19}$$

$$\varepsilon_{rel} = \frac{\left| \varepsilon_{abs} \right|}{A_{true}} \times 100\% \tag{20}$$

where: A_{ex} denotes the area extracted by the algorithm, and A_{true} denotes the actual area.

Table 3

Improved Alpha Shapes, Convex Hull, and Delaunay algorithm extraction for area data analysis

Algorithm	Absolute error/10^{-7}	Absolute error Confidence interval/10^{-6}	Relative error /%	Processing time/10^{-2}
Improved Alpha Shapes (non-normal distribution)	−4.66±455	[-6.08,4.60]	1.3484±0.8470	9.213±1.5229
Convex Hull （Normal distribution）	1580±140	[155.4,161.1]	9.3773±0.8575	6.184±1.0635
Delaunay （Normal distribution）	930±80	[91.23,94.34]	5.4964±0.4397	3.577±0.821

Note: Data that do not follow a normal distribution are presented as median ± IQR, while data that follow a normal distribution are presented as mean ± standard deviation.

It is evident that Alpha Shapes extraction yields the smallest absolute error in area measurement ($-7.40\times10^{-7} \pm 2.69\times10^{-5}$)$m^2$, with the narrowest confidence interval (-6.08×10^{-6} to 4.6×10^{-6}) and the lowest relative error $(13.48 \pm 8.47)\times10^{-3}$, demonstrating high accuracy in area estimation. Its processing time $(9.21 \pm 1.52)\times10^{-2}$s is slightly higher than other methods but remains within an acceptable range. The Convex Hull algorithm exhibited significant underestimation with the highest error levels; the Delaunay algorithm achieved a relatively balanced trade-off between accuracy and efficiency, though its precision fell short of the Alpha Shape method. Considering both error analysis and computational efficiency, the improved Alpha Shapes method proves superior, ensuring accuracy while maintaining feasibility for engineering applications.

CONCLUSIONS

(1) This study proposes a rapid machine-vision algorithm for extracting the area of irregular laser-cladded regions on rotary tiller blades. A comprehensive image-processing workflow was established, integrating grayscale conversion, Gaussian blur noise reduction, OTSU automatic threshold segmentation, and morphological operations with boundary-tracking contour detection and grayscale analysis for bright-region extraction. Through comparative evaluation, an improved Alpha Shapes algorithm was selected for region segmentation, enabling accurate extraction of laser-cladding areas.

(2) Comparative experiments using manually calibrated electron microscope measurements as the reference show that, among the three tested algorithms, the improved Alpha Shapes algorithm provides the highest accuracy. Compared with the Convex Hull and Delaunay triangulation methods, it achieves the smallest absolute error ($-7.40\times10^{-7} \pm 2.69\times10^{-5}$)$m^2$, the narrowest confidence interval (-6.08×10^{-6} to 4.6×10^{-6}) and the lowest relative error $(13.48 \pm 8.47)\times10^{-3}$. The method maintains high precision while offering computational efficiency suitable for industrial applications.

(3) The machine vision approach developed in this study enables efficient, non-contact, and automated extraction of irregular laser-cladding regions on rotary tiller blades, demonstrating strong consistency with electron microscope measurements. This method overcomes the limitations of traditional manual inspection and provides a practical technical solution for laser-cladding quality assessment. Furthermore, it offers potential for extension to related applications such as tool wear monitoring and weld defect detection.

ACKNOWLEDGEMENT

This research was supported by the 2024 Scientific Research Project of the Shaanxi Provincial Department of Education (Project No.: 24JK0508) and the 2025 Educational Teaching Reform Research Project of Xi'an Aeronautical Polytechnic Institute (Project No.: 25XHJG02).

REFERENCES

[1] Al-Khudhairy D.H.A., Caravaggi I., Giada S., (1983). Structural damage assessments from Ikonos data using change detection, object-oriented segmentation, and classification techniques. *Photogrammetric Engineering & Remote Sensing*, Vol. 71, No.7, pp.825-837.

[2] Chan T.F., Vese L.A., (2022). Active contours without edges. *IEEE Transactions on Image Processing*, Vol. 10, No. 2, pp. 266-277.

[3] Ding Y., Bi W., Zhong C., (2022). A comparative study on microstructure and properties of ultra-high-speed laser cladding and traditional laser cladding of Inconel 625 coatings. *Materials*, Vol.15, No.18, pp.6400.

[4] Edelsbrunner H., Kirkpatrick D.G., Seidel R., (1983). On the shape of a set of points in the plane. *IEEE Transactions on information theory*, Vol.29, No.4, pp.551-559.

[5] Haldar B., Saha P., (2018). Identifying defects and problems in laser cladding and suggestions of some remedies for the same. *Materials Today: Proceedings*, Vol. 5, No.5, pp.13090-13101.

[6] Hou S.X., Li Z F., Wu C., Liu H.Y., Zhang H.Q., (2025). Research Status of High Temperature Wear-resistant Coating by Laser Cladding. *Special Casting & Nonferrous Alloys*, Vol.45, No.10, pp.1447-1456, Wu Han/China.

[7] Itti, L., Koch, C., (1999). A Comparison of Feature Combination Strategies for Saliency-Based Visual Attention Systems. *Proceedings of SPIE - The International Society for Optical Engineering*, Vol.3644, No.1 pp.473~482.

[8] Kong X., Everett H., Toussaint G., (1990). The Graham scan triangulates simple polygons. *Pattern Recognition Letters*, Vol. 11, No. 11, pp. 713-716.

[9] Lee D.J., Xu X., Eifert J., Zhan P., (2006). Area And Volume Measurements of Objects With Irregular Shapes Using Multiple Silhouettes. *Optical Engineering*, Vol. 45, No. 2, pp. 027202-027202.

[10] Lee D.T., Lin A.K., (1986). Generalized Delaunay Triangulation for Planar Graphs. D*iscrete & Computational Geometry*, Vol. 1, No. 3, pp. 201-217.

[11] Li C., (2007). *Research on Key Technique of RoI Detection for Static Image（静态图像感兴趣区域提取关键技术研究）*, MA thesis, TIANJING University, Tian Jin/China.

[12] Liu J.M., (2024). Research On Infrared Small Target Detection Algorithm Based On Local Contrast Mechanism (基于局部对比度机制的红外小目标检测算法研究), MA thesis, Xi'an University of Technology.

[13] Lubis S.R., Iqbal, M., (2024). A Study on Implementation and Performance Analysis of Basic and Advanced Image Processing Techniques Using Python and OpenCV. *Journal of Computer Science and Research (JoCoSiR)*. Vol. 2, No.2, pp.21–28. https://doi.org/10.65126/jocosir.v2i2.60.

[14] Lv C., Li Z., Shen Y., Li J., Zheng J., (2022). Separafill: two generators connected mural image restoration based on generative adversarial network with skip connect. *Heritage Science*, Vol. 10, No.1, pp.135.

[15] Minchul K., Hong J., (2025). Automatic extraction of region of interest from images with low depth of field. *IEEE Networking and Information Technology*, pp. 257~259.

[16] Otsu N., (2007). A Threshold Selection Method from Gray-Level Histograms. *IEEE Transactions on Systems, Man, and Cybernetics*, Vol.9, No.1, pp.62-66.

[17] Poloczek T., Lont A. , Górka J., (2022). Structure and properties of laser-cladded Inconel 62 5-based in situ composite coatings on S355JR substrate modified with Ti and C powders. *M aterials Science-Poland*, Vol.40, No.3, pp.1265-1265. https://doi.org/10.2478/msp-2022-0039

[18] Ren M., Yang J., Sun H., (2002). Tracing boundary contours in a binary image. *Image and vision computing*, Vol. 20, No.2, pp.125-131.

[19] Song Y.B., (2022). Leaf Area Measurement System Based on Digital Image Processing Technology (数字图像处理技术在叶面积测量中的应用). *Journal of Agriculture*, Vol. 12, No. 02, pp. 73-75.

[20] Yokoyama M., Poggio T., (2005). A Contour-Based Moving Object Detection and Tracking. *IEEE International Workshop on Visual Surveillance and Performance Evaluation of Tracking and Surveillance*, pp. 271-276.

[21] Zeng Y., Fu J., Chao H., Guo, B., (2021). Aggregated contextual transformations for high-resolution image inpainting. *IEEE Transactions on Visualization and Computer Graphics*.

[22] Zhang J., Hu J., (2008). Image segmentation based on 2D Otsu method with histogram analysis. *international conference on computer science and software engineering. IEEE Computer Society*, Vol.6, pp.105-108.

[23] Zhang Y., Bai P., Li Z., Zhang J., (2025). A review of laser cladding monitoring and control based on the molten pool images. *The International Journal of Advanced Manufacturing Technology*, pp.1-24.

[24] Zhu Q.J., (2018). *Study on the Process Characteristics of Circular Multi-laser Melting Wire Additive Manufacturing (环列式多激光束熔丝增材制造工艺特性研究)*, MA thesis, Chong Qing University.